ESD Behavior of Metallic Carbon Nanotubes

Mayank Shrivastava (1) and Harald Gossner (2)

(1) Department of Electronic Systems Engineering, Indian Institute of Science Bangalore, Bangalore, Karnataka, India
tel.: +91-080-2293-2732, e-mail: mayank@dese.iisc.ernet.in

(2) Intel Corp., Mobile and Communications Group, Am Campeon 12, Neubiberg, Germany

Abstract – ESD behavior of metallic carbon nanotubes (CNTs) is explored. Unique TLP I-V characteristics and failure mechanism of carbon shells are discussed. ESD failure in CNTs is attributed to shell burning. It was found that CNT interconnect changes resistance in steps of fundamental quantum resistance ($h/2e^2$) after individual shell burning.

I. Introduction

Carbon based nano materials like Carbon nanotubes (CNTs) have become a focus material for beyond CMOS transistor and interconnect technologies [1]-[4]. Physics of carrier transport under low and high electric fields, quantum conductance, and thermal failure in CNTs have been extensively studied for quasi-static operation [5]-[6]. However, Electrostatic discharge (ESD) behavior of CNTs is widely unknown except a recent work on Multiwalled CNTs [7]. This work analyses the ESD/TLP behavior and the novel ESD failure mechanism of CNTs interconnects towards the development of a useful ESD failure model.

II. Carbon Nanotubes

Carbon Nanotubes (CNTs) are members of the fullerene structural family of carbon allotropes and are cylindrical in shape. CNTs have two families, namely single wall carbon nanotube (SWCNT) and multiwall carbon nanotube (MWCNT), and are of three different types, i.e. *chiral*, *armchair* and *zigzag*. They can be conceptually seen as cylindrical wrapping of monolayer Graphene (a single layer of graphite). SWCNT is a hollow tube of carbon atoms conceptually formed by wrapping of monolayer Graphene arranged in a hexagonal (honeycomb like) lattice and composed entirely of sp^2 bonds. MWCNT, however, is a concentric cylindrical structure of multiple SWCNTs (Fig. 1). The SWCNT or individual SWCNT tubes of a MWCNT can be of *chiral*, *armchair* or *zigzag* nature.

Figure 2 depicts wrapping of Graphene monolayer to form CNTs. The shaded regions (Fig. 2i & 2ii) show the wrapping plane and portion of Graphene monolayer which forms CNTs. CNT's electrical properties depend on the chiral vector C_h, where: $C_h = na_1 + ma_2 = (n, m)$, ($n$, m are positive integers and $0 \leq m \leq n$); diameter (d) of the tube, which is derived from the chiral vector $|C_h|$: $d = \sqrt{C_h \cdot C_h/\pi}$ and angle ϕ ($cos\emptyset = C_h \cdot a_1/|C_h||a_1|$), which is angle between chiral vector and lattice vector a_1. *Zigzag* tubes have $\phi = 30^o$ (Fig. i) and *armchair* tubes have $\phi = 0^o$ (Fig. ii), whereas *chiral* tubes have $0 < \phi < 30^o$. A CNT is metallic if ($n - m$) is an integer multiple of 3 or 0, otherwise it is semiconducting.

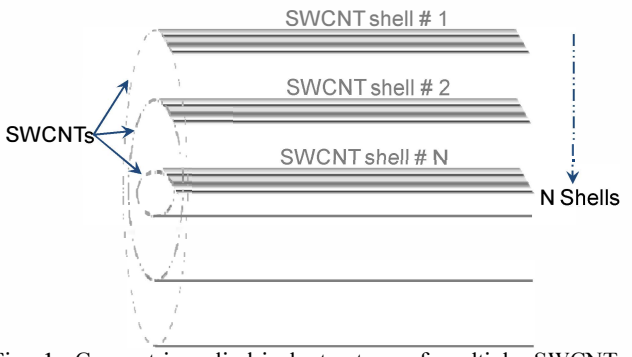

Fig. 1: Concentric cylindrical structure of multiple SWCNTs, which forms MWCNT.

Typically SWCNT's diameter ranges from 0.5nm to 5nm. MWCNTs can have diameter up to 100nm. The minimum spacing between individual SWCNTs in a MWCNT is 3.4 Å. Typically MWCNT have 2/3rd metallic SWCNTs and 1/3rd semiconducting SWCNTs. Therefore, in general, MWCNTs are metallic in nature.

Another interesting property of CNTs is related to its band structure. CNTs have multiple subbands at higher energies (number of subbands increases with CNT's diameter). Moreover, CNTs have symmetric band structure, especially at low energies, i.e. high electron-hole symmetry at low energies. Finally, bandgap (E_g) of semiconducting CNTs is inversely proportional to its diameter using relation E_g (eV) ~ 0.9/*d* (nm). Fig. 3a and 3b depict the band bending in metallic and semiconducting CNTs respectively. Both Fig. 3a and 3b show the high energy subbands and electron-hole symmetry. Fig. 3a shows zero bandgap, whereas Fig. 3b shows a finite bandgap (E_g). In this work MWCNTs are used for ESD exploration.

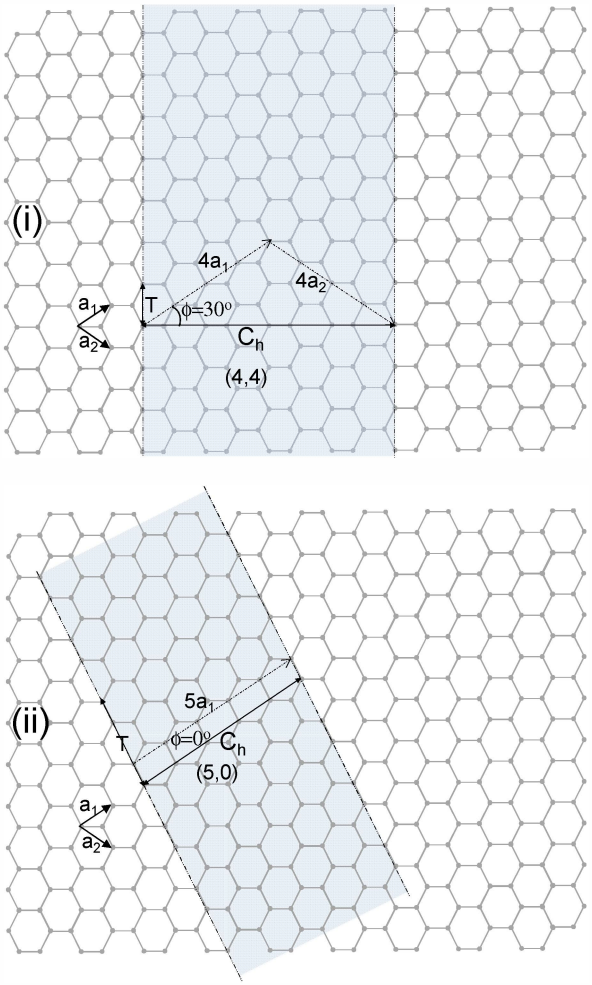

Fig. 2: (i) Wrapping of Graphene monolayer to form an *armchair* SWCNT (ii) Wrapping of Graphene monolayer to form a *zigzag* SWCNT.

III. Device Under Test

MWCNTs for ESD investigations were grown by thermal CVD method. For CVD growth a mixture of ferrocene and toluene at a temperature of 850 °C was used. Thereafter, grown tubes were detached from the substrate and then dispersed individually on top of 250nm thick Cr/Au contact pads. Cr/Au contact pads were deposited and patterned over a Si/SiO_2 substrate (thermally grown SiO_2 over a Si substrate). Spacing between individual metal pads was 2µm (Fig. 4). Note that the CNTs under tests are suspended between metal pads.

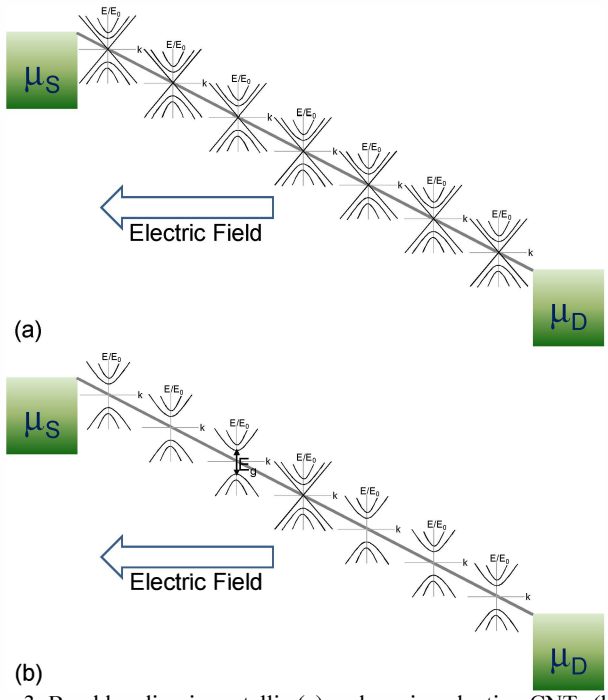

Fig. 3: Band bending in metallic (a) and semiconducting CNTs (b) depicting high energy subbands, electron-hole symmetry and respective bandgap.

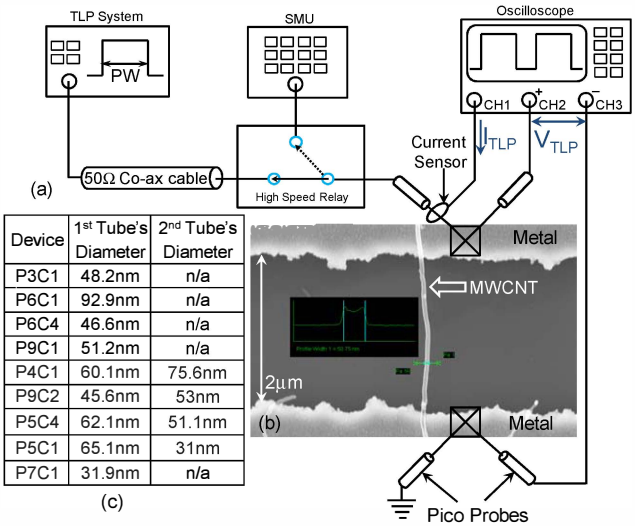

Device	1st Tube's Diameter	2nd Tube's Diameter
P3C1	48.2nm	n/a
P6C1	92.9nm	n/a
P6C4	46.6nm	n/a
P9C1	51.2nm	n/a
P4C1	60.1nm	75.6nm
P9C2	45.6nm	53nm
P5C4	62.1nm	51.1nm
P5C1	65.1nm	31nm
P7C1	31.9nm	n/a

(c)

Fig. 4: (a) A 4 probe, very fast transmission line pulsing setup, (b) SEM image of one of the CNT sample under test and (c) list of test structures with respective tube's diameter. Note that some of the test structures have two CNTs dispersed between the metal pads. After each pulse stress, tube's resistance (R) was extracted at a low DC voltage.

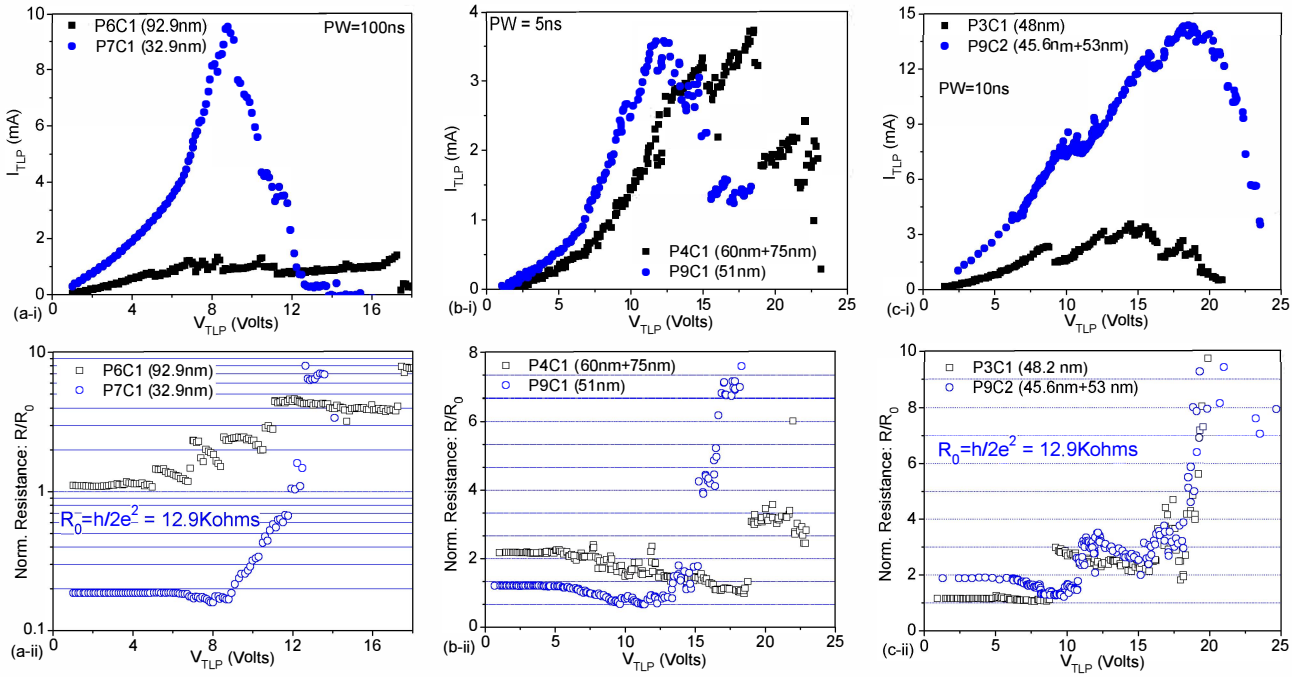

Fig. 5: (a-i, b-i and c-i) TLP I-V characteristics of various metallic CNT samples stressed under 100ns, 5ns and 10ns TLP stress. (a-ii, b-ii and c-ii) CNT tube's resistance at low bias, extracted after each stress pulse during TLP test, in the units of fundamental quantum resistance.

IV. TLP I-V Characteristics

Fig. 5 shows TLP I-V characteristics of 6 different CNT samples stressed using 100ns, 5ns and 10ns TLP pulses, respectively. After each stress/TLP pulse, tube's resistance was extracted in the units of fundamental quantum resistance (R_0),

$$R_0 = \left(\frac{h}{2e^2}\right) \quad (1)$$

where h is plank's constant and e is electron charge. Fig. 5 shows that CNTs under ESD test have pre-fail resistances in a range of $0.1R_0$ to $2R_0$, which has no correlation with their respective diameters. Fig 5 shows distinct TLP I-V relationship at high currents. A clear metallic (linear I-V) behavior can be seen from various TLP I-V plots at lower voltages; however, CNT changes its behavior at high currents and fields. For example, P6C1 (see details of sample in Fig. 4c) under 100ns TLP stress shows a liner relation till the first fail, however, P7C1 shows an exponential relation after 4V (see Fig. a-i). Exponential I-V relation at higher voltages can be attributed to band-to-band tunneling between non-crossing energy bands. Interestingly, P6C1 has a quantized (step like, in multiples of R_0) increase in tube's resistance after each fail, however P7C1 shows a gradual increase in tube's resistance (see Fig. 5a-ii). Other clear difference can be observed in terms of current handling capacity of P7C1. Despite of ~3× smaller diameter, P7C1 can carry ~10× more current that P6C1.

A similar I-V behavior can be observed from other samples P4C1, P9C1 (Fig. 5b-i and 5b-ii) and P3C1, P9C2 (Fig. 5c-i and 5c-ii) stressed under 5ns and 10ns TLP. P9C1 and P4C1 show initially a linear I-V relation, which changes to exponential relationship at higher TLP voltages. Moreover, both the samples (with tube's resistance > R_0) show a step like drop in current and quantized increase in resistance after each fail. Exponential I-V relation at higher bias can also be attributed to filling of high energy states in these materials. For clarity and statistical justification of arguments presented above, few more samples (P5C4, P5C1 and P6C4) were stressed using TLP (pulse widths = 20ns, 50ns and 500ns, respectively). Their respective TLP I-V behaviors are depicted in Fig. 6, which adds to the explanations given above.

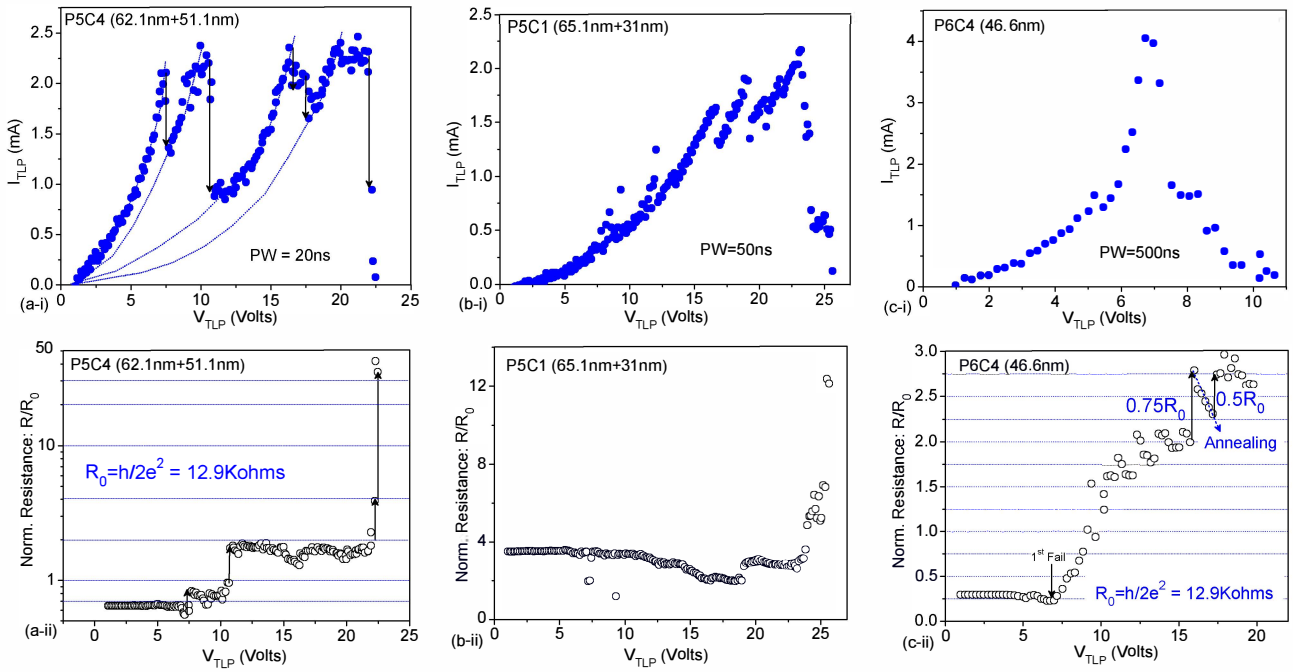

Fig. 6: (a-i, b-i and c-i) TLP I-V characteristics of various metallic CNT samples stressed under 20ns, 50ns and 500ns TLP stress. (a-ii, b-ii and c-ii) CNT tube's resistance at low bias, extracted after each stress pulse during TLP test, in the units of fundamental quantum resistance.

In general, all the samples under test conduct at all TLP voltages, and undergo into the failure mode at higher voltages. Unlike to metals in which ESD/TLP current drops immediately after the (first) fail, metallic CNTs show a gradual or step like drop in current. Moreover, after each failure tube's resistance either changes gradually or in steps of fundamental quantum resistance ($R_0=h/2e^2$). This behavior can be linked with the geometry or tube's arrangement in MWCNTs (discussed in the next section). It's worth highlighting an observation that most of the tube's with resistance < R_0 give rise to an exponential increase in current at higher TLP voltages, moreover, such tube's fail with a gradual drop in current. On the other hand, tubes with resistance > R_0 mostly show a linear I-V relation till the first failure (burning of outer shell) and current drops in steps with the failure/burning of each shell.

A comparison of failure current (It2, @ first fail) of different samples (P9C1, P3C1 and P6C1) with comparable tube's resistances (~ R_0, at low bias) and stressed under different TLP pulse widths (5ns, 10ns and 100ns respectively) show a power law like relation ($here\ It2 \sim t^{-n}, where\ n < 0.2$), i.e. It2 falls with increasing pulse width (3.4mA, 2.3mA and 1.1mA respectively). Similarly, tubes (P7C1 and P6C4) with resistance < R_0 (~$0.2R_0$) show a power like behavior. It's worth highlighting that comparison of It2 must be done for tubes with comparable resistance (extracted at low bias). Unfortunately, a comparison in terms of It2 per unit diameter is not

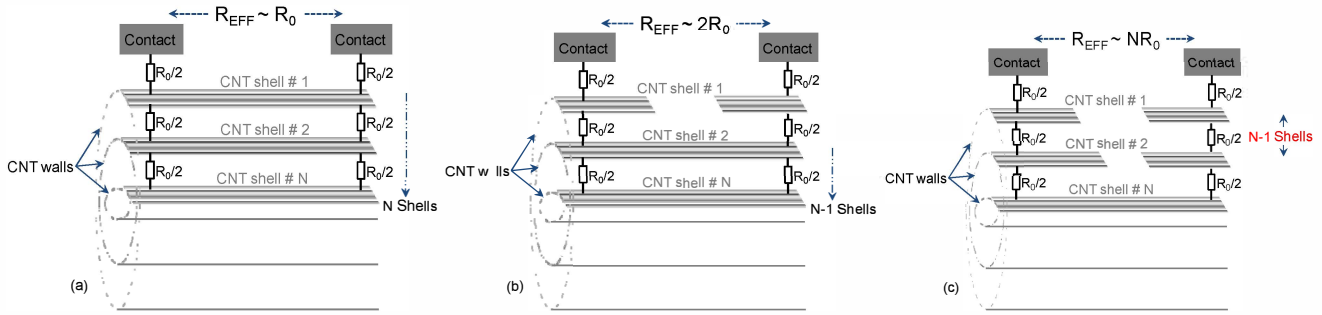

Fig. 7: A model depicting a possible way of coupling between metal pads and CNT shells and explaining step change in resistance after each fail. (a) Figure shows a possible way of CNT shell to contact coupling of a virgin device. (b-c) Show how a quantized change in tube's resistance is possible after 1st and (N-1)th fail. (A 3D illustration of shell burning is also given in Fig. 7b).

possible given that each tube may have different number of shells available for current conduction, which is attributed to immaturity of the state-of-the-art CNT growth process available.

V. Failure Analysis

In this section ESD failure behavior of CNT samples is discussed. However, before explaining failure behavior, we have tried to develop a generalized model for the quantized change in resistance after each fail (seen as a fall in I-V characteristics). Fig. 7a shows a possible way of contacting (coupling) between CNT shells and metal pads. MWCNTs have multiple concentric shells (also depicted in Fig. 10b). The model shows N groups of CNT shells, each group consists of one or more CNT shells. Fig. 7b and 7c show two extreme cases after failure and respective effective tube's resistance, depicting the quantized change in resistance. It's worth pointing that increase of tube's resistance does not result from degrading contacts. It is due to removal of single carbon layers, which is a novel failure mechanism. This is proven by the location of the final fail in the center of the CNT tube as shown in SEM images (Fig. 8). Fig. 8 shows: (i) damage location was often found to be at the center position, which can be attributed to thermal failure of diffusive CNTs, and (ii) no carbon left over can be seen at the failure site, i.e. carbon materials have no molten state.

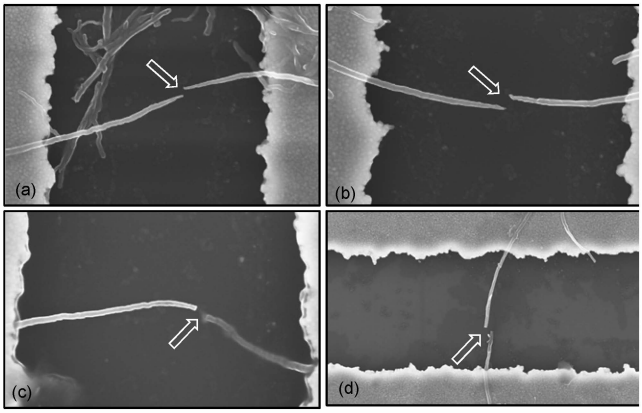

Fig. 8: Figure shows various CNT samples damaged after ESD stress. Damage location was often found to be at the center along the length of the tube.

Failure at the center (i) can be explained using diffusive carrier transport, in which carrier travelling from one terminal to the other uniformly loses its energy across the channel (here CNT). As the center of tube will see highest thermal resistance, this region will gain the maximum heat (location of hot spot) and therefore will burn first. Later (ii) can be explained as loss of carbon due to oxidation under extreme stress (thermal) conditions, which is also evident from Fig. 9 and 10. Fig. 9-10 shows thinning of carbon nanotube close to the damage site, Fig. 9(a) shows SEM image of a virgin tube with diameter of 47.35nm, which was reduced to 28.32nm after ESD damage as shown in Fig. 9b.

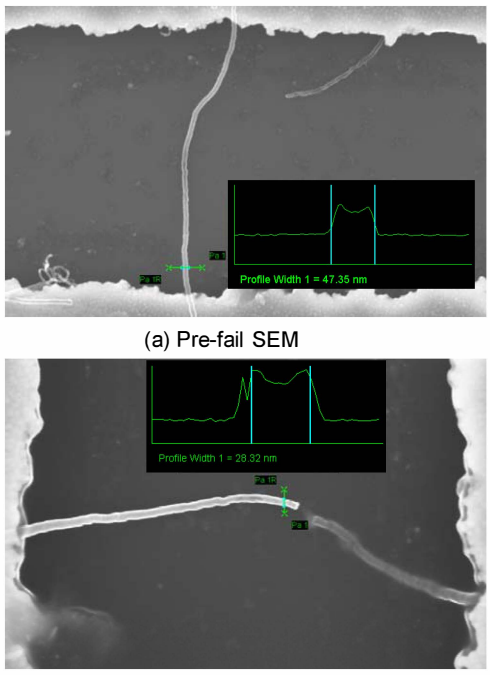

Fig. 9: Thinning of carbon nanotube close to the failure point validating loss of carbon material under ESD stress. (a) SEM image of virgin device with tube's diameter of 47.35nm. (b) SEM image of damaged tube with reduced diameter (28.32nm) close to the failure point.

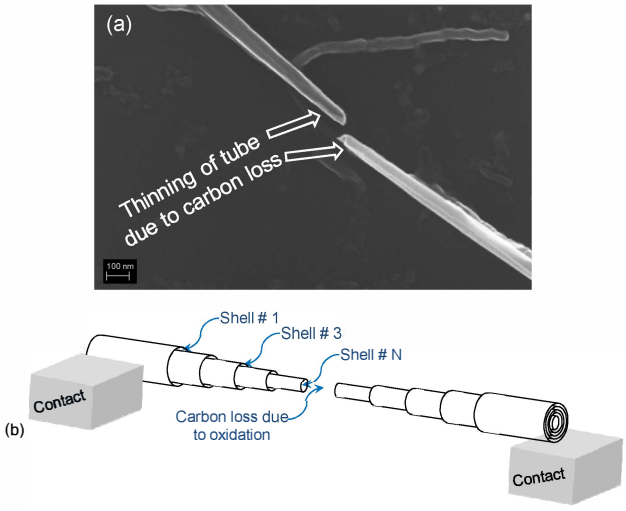

Fig. 10: (a) A closer view of failure location in one of the CNT sample, clearly depicting reduced tube's diameter and loss of carbon next to failure point. (b) A pictorial representation of the same.

VI. Conclusion

ESD behavior of metallic (Multiwalled) CNT interconnects was explored and found to be different from metals. For example, step-by-step destruction of individual shells with increasing pulse amplitude was seen. Moreover, a quantized increase in tube's resistance in the units of $h/2e^2$ was observed. The quantized increase in tube's resistance is used to model a possible scheme for CNT-to-metal contact. Finally, it was found that carbon materials fail due to oxidation of carbon under extreme stress (thermal) conditions.

References

[1] H. Li, et. al, "Carbon Nanomaterials for Next-Generation Interconnects and Passives: Physics, Status and Prospects," IEEE Transactions on Electron Devices, vol. 56, no. 9, pp. 1799-1821, 2009.

[2] N. Srivastava, et. al, "On the Applicability of Single-Walled Carbon Nanotubes as VLSI Interconnects," IEEE Transactions on Nanotechnology, vol. 8, no. 4, pp. 542-559, 2009.

[3] A. D. Franklin, et. al., "Scalable and fully self-aligned n-type carbon nanotube transistors with gate-all-around", IEEE IEDM 2012.

[4] Ji Cao, et. al., "Large-scale assembly of tunable resonant-body carbon nanotube transistors without hysteresis", IEEE IEDM 2012.

[5] A. Urbina, et. al., "Quantum Conductance Steps in Solutions of Multiwalled Carbon Nanotubes," Physical Review Letters, vol. 90, no. 10, pp. 12-15, Mar. 2003.

[6] P. G. Collins, et al., "Current Saturation and Electrical Breakdown in Multiwalled Carbon Nanotubes," Physical Review Letters, vol. 86, no. 14, pp. 3128-3131, 2001.

[7] Mayank Shrivastava, et. al., "ESD Investigations of Multiwalled Carbon Nanotubes," IEEE Transactions on Device and Materials Reliability, Vol. 14, No. 1, March 2014, pp: 555 – 563.